

# Highly Ordered BN<sub>⊥</sub>–BN<sub>⊥</sub> Stacking Structure for Improved Thermally Conductive Polymer Composites

Barun Ghosh,\* Fang Xu, David M. Grant, Paolo Giangrande, Chris Gerada, Michael W. George, and Xianghui Hou\*

The substantial heat generation in modern electronic devices is one of the major issues requiring efficient thermal management. This work demonstrates a novel concept for the design of thermally conducting networks inside a polymer matrix for the development of highly thermally conductive composites. Highly ordered hexagonal boron nitride (hBN) structures are obtained utilizing a freeze-casting method. These structures are then thermally sintered to get a continuous network of BN<sub>⊥</sub>–BN<sub>⊥</sub> of high thermal conductivity in which a polymer matrix can be impregnated, enabling a directional and thermally conducting composite. The highest achieved thermal conductivity ( $K$ ) is  $4.38 \text{ W m}^{-1} \text{ K}^{-1}$  with a BN loading of 32 vol%. The effect of sintering temperatures on the  $K$  of the composite is investigated to optimize connectivity and thermal pathways while maintaining an open structure (porosity  $\approx 2.7\%$ ). The composites also maintain good electrical insulation (volume resistivity  $\approx 10^{14} \Omega \text{ cm}$ ). This new approach of thermally sintering BN<sub>⊥</sub>–BN<sub>⊥</sub> aligned structures opens up a new avenue for the design and preparation of filler alignment in polymer-based composites for improving the thermal conductivity while maintaining high electrical resistance, which is a topic of interest in electronic packaging and power electronics applications.

## 1. Introduction

The drive to ever-increasing power density requirements and complex 3D integration of components and systems in electrical devices is severely limited by thermal management issues. Undissipated heat reduces lifetime and efficiency of the devices significantly,<sup>[1]</sup> thus requiring the use of materials tailored to promote efficient thermal management ensuring the operating temperature is maintained within its functional range. In particular, there is a need for cost-effective, thermally conductive materials with a high electrical resistance. The design of such materials is based on highly thermally conductive fillers reinforced into polymer matrix and applied as thermal interface materials (TIMs) to reduce the interface resistance between the heat sink and the point of heat generation. To date, many studies have claimed that metals and carbon-based fillers such as graphene,<sup>[2,3]</sup>


carbon nanotubes (CNTs),<sup>[4,5]</sup> graphite flakes<sup>[6]</sup> can be used as highly thermally conducting fillers to improve the thermal conductivity of polymer-based composites. Although carbon-based composites exhibit excellent thermal properties, they possess electrical conductivity, resulting in current leakage that limits the practical application of these composites.<sup>[7,8]</sup> Thus, ceramic particles such as boron nitride (BN),<sup>[9–11]</sup> aluminium nitride (AlN),<sup>[12,13]</sup> silicon carbide (SiC)<sup>[14,15]</sup> are often used as thermally conductive and electrically insulating fillers to realize TIMs when incorporated in to power electronic devices. The formation of continuous thermally conducting paths by a controllable alignment of fillers inside composite is an effective method to improve the thermal conductivity of TIMs along a certain direction at low loading. Substantial efforts have been devoted to align the fillers, especially for anisotropic materials like BN into the composite using different strategies such as electrospinning,<sup>[16,17]</sup> stretching,<sup>[18]</sup> doctor blading<sup>[19]</sup> induced by magnetic field,<sup>[20–22]</sup> electric field,<sup>[23,24]</sup> gravitational force field,<sup>[25,26]</sup> and 3D printing technology.<sup>[27]</sup> Freeze-casting method is also a promising approach to form highly ordered structures of fillers inside the composite. The fillers are aligned along the ice crystal growth direction, and a small amount of fillers can build continuous thermally conductive networks inside the composite. Hu et al.<sup>[28]</sup> and Zeng et al.<sup>[29]</sup> developed thermally conducting

Dr. B. Ghosh, Dr. F. Xu, Prof. D. M. Grant, Dr. X. Hou  
Advanced Materials Research Group, Faculty of Engineering  
University of Nottingham  
Nottingham NG7 2RD, UK  
E-mail: barun.ghosh@nottingham.ac.uk; xianghui.hou@nottingham.ac.uk

Dr. P. Giangrande, Prof. C. Gerada  
Power Electronics, Machines and Control (PEMC) Group  
Faculty of Engineering  
University of Nottingham  
Nottingham NG7 2RD, UK

Prof. M. W. George  
School of Chemistry  
University of Nottingham  
Nottingham NG7 2RD, UK

Prof. M. W. George  
Department of Chemical and Environmental Engineering  
University of Nottingham Ningbo China  
199 Taikang East Road, Ningbo 315100, China

 The ORCID identification number(s) for the author(s) of this article can be found under <https://doi.org/10.1002/aelm.202000627>.

© 2020 The Authors. Published by Wiley-VCH GmbH. This is an open access article under the terms of the Creative Commons Attribution License, which permits use, distribution and reproduction in any medium, provided the original work is properly cited.

DOI: 10.1002/aelm.202000627

composites using the freeze-casting method to construct interconnected networks of BN in epoxy resin.

The interfacial thermal resistance is another key factor affecting the thermal conductivity of polymer composite. It forms a barrier for phonon transport and prevents thermal conduction. This resistance originates from the filler/filler and filler/polymer interface and comes from two aspects: 1) mismatch in the vibrational energy between the inorganic and polymer phase; and 2) weak interfacial adhesion and physical contact and between the filler and matrix. Composites, without any evident filler alignment, experience a much higher interfacial thermal resistance resulting in decreased conductivity.<sup>[28,29]</sup> For example, Zeng et al.<sup>[29]</sup> reported in their studies that the interfacial resistance in epoxy/BN aligned composites was two orders of magnitude smaller than epoxy/BN random composites. Thus, it is important to minimize the interfacial thermal resistance of polymer composite as much as possible to construct a continuous filler network.<sup>[30]</sup> In a polymer composite where thermally conductive fillers are considered as conduction promoters and filler/polymer interfaces as gaps, phonons jump from one filler to another to cross the polymer matrix, and thus require a longer time to conduct heat. The construction of a continuous expressway with as few gaps as possible could be an efficient approach to transfer heat effectively by minimizing the interfacial thermal resistance. High-temperature sintering of aligned structures of fillers is a novel concept adopted here to minimize the interfacial thermal resistance by forming an elaborated filler–filler diffused interface, where phonons can easily pass through with reduced scattering. The sintered junctions will provide much stronger interactions, leading to strong mechanical strength of the composites. Sintering also ensures the continuity of thermally conducting paths inside the composites. The introduction of a sintering phase can cross-link adjacent filler platelets, which can improve the interfacial adhesion with the matrix.<sup>[31–33]</sup> It was reported that silver nanoparticles reduce the thermal interfacial resistance after sintering within BN structures when used as a thermal transport junction.<sup>[34]</sup> However, this leads to the risks of electro-migration.<sup>[34,35]</sup>

This present work is aimed at developing an approach that can lead to a step-change electrical insulating material with significantly improved thermal dissipation capability. Our approach is based upon the concept of constructing heterostructure thermal conduction pathways/skeletons followed by the impregnation/curing of polymer matrices. We demonstrate a concept for designing thermally conducting networks based on BN micro-platelets inside a polymer matrix, for the development of highly thermally conductive composites. The addition of BN nanoparticles was proposed to minimize this risk of electromigration when used as thermal transport junction, which could also join the gaps between BN micro-platelets to make continuous heat-conducting networks, providing a significant contribution to the enhancement in thermal conductivity. To verify this hypothesis, hBN platelets of different diameters ( $\approx 70$  nm and  $\approx 5$   $\mu\text{m}$  and  $30$   $\mu\text{m}$ ) were used as fillers in this work. hBN exhibits high thermal stability of up to  $1000$   $^{\circ}\text{C}$  in air and  $1400$   $^{\circ}\text{C}$  in vacuum, high electrical insulation, and extremely high thermal conductivity ( $600$   $\text{W m}^{-1} \text{K}^{-1}$  for in-plane direction,  $K_{\perp}$ ), and  $30$   $\text{W m}^{-1} \text{K}^{-1}$  along through-plane direction,

$K_{\perp}$ ). The alignment of BN platelets was achieved by a combination of freeze-casting followed by thermally sintered at  $1000$   $^{\circ}\text{C}$  to obtain  $\text{BN}_{\perp}$ – $\text{BN}_{\perp}$  diffused interface. A liquid epoxy resin was subsequently impregnated into BN–BN stacking structures under vacuum to obtain the desirable composite. The surface morphology, microstructural information, and thermal properties were systematically investigated for the aligned epoxy/BN composites with different hBN loadings and sintering temperatures and the results were compared with randomly mixed BN composites. The effect of different sintering temperatures on the thermal properties was also examined. The developed composites in this work have potential as heat-dissipating materials for electronic packaging and power electronics applications.

## 2. Results and Discussion

**Figure 1** presents a schematic illustration for the production of highly ordered  $\text{BN}_{\perp}$ – $\text{BN}_{\perp}$  stacking structures and the corresponding composite development process. The aligned BN structures were obtained by a freeze-casting method followed by high-temperature sintering to develop a continuous and diffused  $\text{BN}_{\perp}$ – $\text{BN}_{\perp}$  interface and finally a liquid epoxy impregnation under vacuum was performed to derive the composites. **Figure 2a–d** shows the cross-sectional scanning electron microscopy (SEM) images of highly aligned BN platelets ( $\approx 5$   $\mu\text{m}$ ) before sintering, after sintering at  $600$   $^{\circ}\text{C}$ , epoxy/aligned BN composite (2.6 vol%), and epoxy/random BN composite (2.6 vol%), respectively. All the aligned BN structures are porous and highly anisotropic along the freezing direction, as shown in **Figure 2a**. Further SEM images of the porous and highly aligned hBN structures are provided in the supporting information (**Figure S1**, Supporting Information). Even after thermal annealing at  $600$   $^{\circ}\text{C}$ , the structure was well maintained, and the vertical alignment of platelets remaining apparently unchanged (**Figure 2b**). The cross-sectional SEM image of epoxy/BN composite (**Figure 2c**) shows the alignment of BN platelets along the ice crystal growth direction. The liquid epoxy was successfully impregnated into the BN scaffolds under vacuum and maintained the ordered structures. The surface morphology of epoxy/random BN composite (**Figure 2d**) was quite different from the aligned composite as the platelets were randomly distributed throughout the matrix.

To further verify the alignment of BN in the epoxy matrix, X-ray diffraction (XRD) analysis was carried out. **Figure 2e** shows the XRD patterns of pure BN platelets ( $\approx 5$   $\mu\text{m}$ ), epoxy/random BN composite (2.6 vol%), and epoxy/aligned BN composite (2.6 vol%). The characteristic peaks located at  $2\theta \approx 26.79^{\circ}$ ,  $41.68^{\circ}$ ,  $50.26^{\circ}$  and  $55.18^{\circ}$  correspond to the reflection from (002), (100), (102), and (004) plane, respectively, of hexagonal BN. The observed peak intensities were different in pure BN, epoxy/random BN, and epoxy/aligned BN composites. The horizontally and vertically aligned hBNs are responsible for the reflection from (002) and (100) plane,<sup>[19]</sup> respectively, which is indicated in the upper inset of **Figure 2e**. The relative intensity ( $I$ ) of (100) peak to the sum of the relative intensities of (002) and (100) peaks gives the values of degree of orientation ( $\delta$ ) of hBN along the  $z$ -direction (parallel to the ice growth direction) in the composite.<sup>[36]</sup> All the peaks were normalized with respect

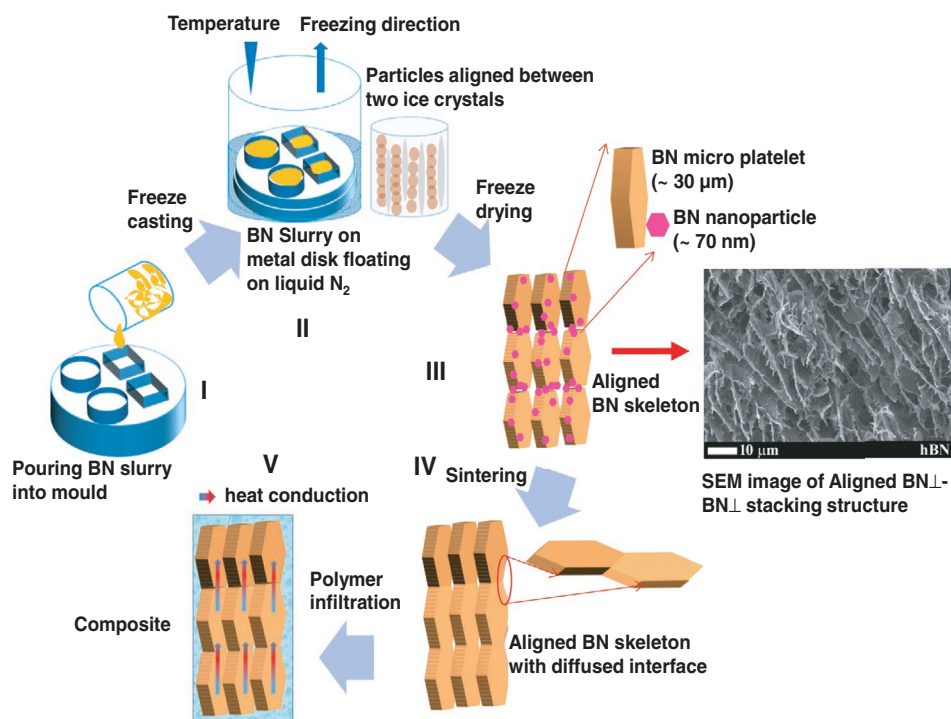


**Figure 1.** Schematic illustrations of the preparation of epoxy/BN composites. I) Preparation and pouring of aqueous slurry containing BN platelets and polyvinyl alcohol (PVA) into a mold; II) freezing of aqueous suspension to form the ice crystals along the temperature gradient; III) freeze-drying to remove the ice and obtain porous BN aligned structures (a typical cross-sectional SEM image of such aligned hBN structure is shown); IV) sintering these ordered structures to develop a continuous and diffused BN<sub>⊥</sub>-BN<sub>⊥</sub> interface; and finally V) a liquid epoxy infiltration under vacuum to derive the composites.

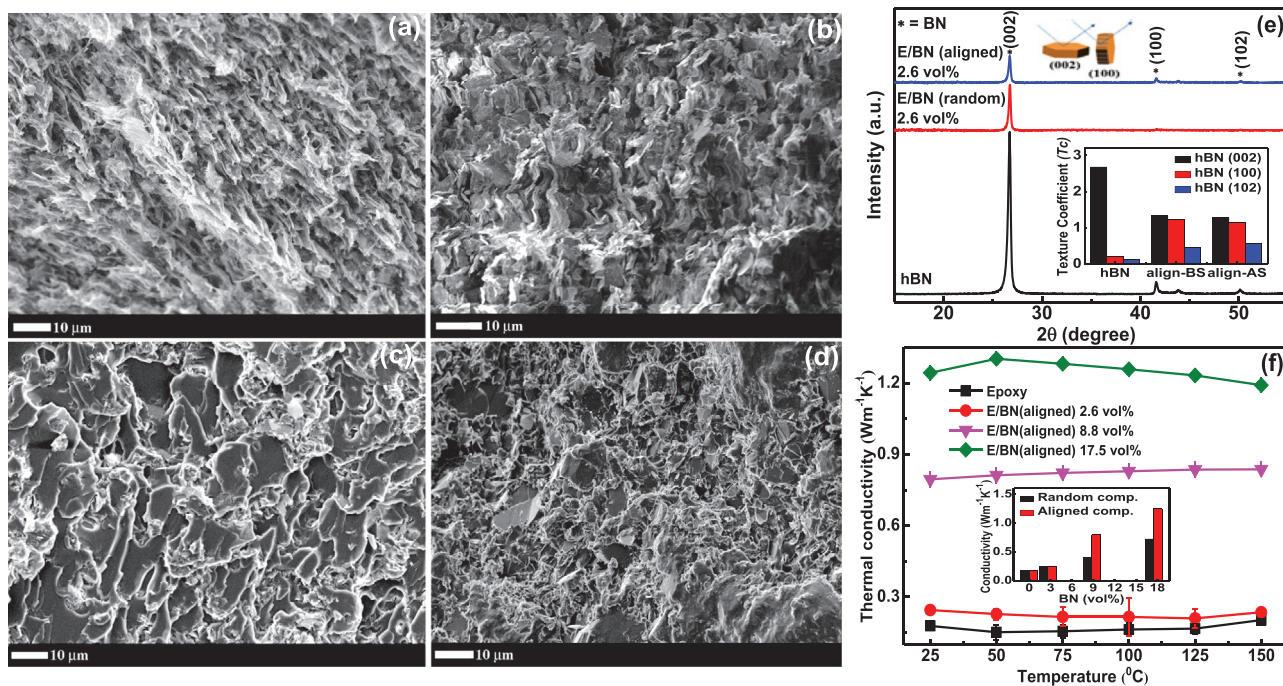


**Figure 2.** Cross-sectional SEM image of BN aligned structures a) before sintering and b) after sintering at 600 °C using 5 μm BN platelets. Cross-sectional SEM image of c) epoxy/BN aligned composite (2.6 vol% BN loading) and d) epoxy/BN random composite (2.6 vol% BN loading). e) XRD patterns of pure BN, epoxy/random BN (2.6 vol%), and epoxy/aligned BN (2.6 vol%) composite; upper inset of (e) shows the illustration of the effect of BN orientation on the XRD pattern, and lower inset of (e) shows texture coefficient (Tc) analysis of BN platelets, BN aligned structures before and after sintering calculated from relative intensity values, and XRD peak data. f) Thermal conductivity (K) as a function of temperature of pure epoxy and epoxy/BN aligned composites with three different BN loading when aligned structures were sintered at 600 °C; inset of (f) shows the comparison of K between the epoxy/aligned BN and epoxy/random BN composites at different BN loadings at 25 °C.

to the reference peak (002). The  $\delta$  value was 6.7% for pure hBN, and 2.8% for random composite, which was increased to 13.7% for aligned composite. This enhancement of  $\delta$  value in aligned composite confirms the increased degree of orientation and favorable alignment of hBN platelets along the ice crystal growth direction, i.e., along (100) diffraction plane. To further investigate the alignment of hBN platelets, texture coefficients (Tc) for pure BN platelets,  $\text{BN}_{\perp}$ - $\text{BN}_{\perp}$  aligned structures before sintering (BS) and after sintering (AS) along three diffraction planes, i.e., (002), (100), and (102), were calculated and shown in lower inset of Figure 2e. The Tc of the plane specified by Miller indices ( $hkl$ ) of  $n$  ( $n$  being the number of peaks calculated; in this case  $n = 3$ ) would indicate preferred orientation along a particular plane.<sup>[37]</sup> For pure BN platelets, as seen from the inset of Figure 2e, the crystalline structure was preferentially oriented along (002) plane, with a  $\text{Tc}_{(002)} = 2.68$ . This value reduced to 1.33 in aligned BN structures, showing a subtle shift of preferred orientation towards (100) plane as  $\text{Tc}_{(100)}$  increased from 0.21 to 1.22. The  $\text{Tc}_{(100)}$  of aligned structures after sintering was similar to the  $\text{Tc}_{(100)}$  of aligned structures before sintering, thus consistent with the stable orientation of BN platelets along (100) plane after sintering.

Figure 2f shows the thermal conductivity as a function of temperature of the aligned composites with three different BN loadings along with pure epoxy. The neat epoxy exhibited a  $K$  value of  $0.18 \text{ W m}^{-1} \text{ K}^{-1}$  at  $25 \text{ }^{\circ}\text{C}$ , which agrees well with the reported  $K$  value of pure epoxy.<sup>[29]</sup> The composites revealed much higher  $K$  values, as the BN loading increased, and this was due to the higher contribution of thermal transport through aligned BN platelets. In particular, the thermal conductivity of epoxy/aligned BN composite was  $1.25 \text{ W m}^{-1} \text{ K}^{-1}$  at 175 vol% BN loading at  $25 \text{ }^{\circ}\text{C}$ ; thus, an enhancement of almost 600% in thermal conductivity was achieved compared to pure epoxy. The thermal stability of all the composites was also investigated in a typical operating temperature range from  $25$  to  $150 \text{ }^{\circ}\text{C}$ . In a disordered material like epoxy resin, thermal conductivity can increase with temperature as a result of better phonon transmission through the interfaces and the decreasing Kapitza resistance at a higher temperature.<sup>[28]</sup> The glass transition temperature ( $T_g$ ) exerts a detectable influence on the thermal conductivity of epoxy. In the glassy state region,  $K$  increases with temperature due to the increase in specific heat, since phonon mean free path is considered practically constant with temperature.<sup>[38]</sup> Even encountering the interfaces of filler-filler or resin-filler, kinetic energy equipped phonons get easier to cross the barriers and an increased thermal conductivity is obtained. In the rubbery state, a decrease in thermal conductivity is observed due to molecular mobility, since in the neighborhood of  $T_g$ , the polymer passes from a rigid and brittle glassy state to the soft rubbery state, where chain segments undergo intensive thermal motion and torsional rotations. This disorder introduced in the structure contributes to the scattering center of phonons (Umklapp scattering)<sup>[39]</sup> and, thereby, decreases the thermal conductivity since phonon Umklapp scattering decreases Kapitza resistance. This was more prominent in the developed composites, especially at higher BN loadings (175 vol% in Figure 2f). Here, the conductivity increased up to  $55 \text{ }^{\circ}\text{C}$  and then decreased with a further rise in temperature. Most of the electronic devices operate at elevated temperatures,

and higher conductivity at elevated temperature can improve heat dissipation. The inset of Figure 2f shows the comparison of thermal conductivity between the random composite and aligned BN composite at different BN loading at  $25 \text{ }^{\circ}\text{C}$ . At all BN loadings, aligned composites had much higher thermal conductivity than random BN composites. The thermal conductivity of epoxy/random BN composite at 175 vol% was  $0.72 \text{ W m}^{-1} \text{ K}^{-1}$  whereas it was  $1.25 \text{ W m}^{-1} \text{ K}^{-1}$  for epoxy/aligned BN composite; thus, an enhancement of 73% in thermal conductivity was reached in the aligned composite compared to the random composite at 175 vol% BN loadings. This improvement was due to the formation of efficient thermally conducting pathways made by BN platelets oriented parallel to the heat flux. To examine the dimensionality and thermal reliability of the composite, the effects of random BN loading and aligned BN loading on CTE were also studied and given in detail in the Supporting Information (Figure S2, Supporting Information). The slightly lower CTE value in the aligned composite also confirmed the well-aligned BN structures stabilizing the whole framework of the composites.

To further improve the thermal conductivity of the composite, a novel concept to form diffused and elaborated  $\text{BN}_{\perp}$ - $\text{BN}_{\perp}$  stacking structures was investigated by sintering the aligned BN structures at different temperatures, i.e., from  $1000$  to  $1200 \text{ }^{\circ}\text{C}$ . Figure 3a,c,e shows the cross-sectional SEM images of the BN aligned structures after sintering at  $1000$ ,  $1100$ , and  $1200 \text{ }^{\circ}\text{C}$ , respectively. The high-resolution images at the BN-BN interface after sintering are illustrated in Figure 3b,d,f, respectively. In the heat treatment process, BN platelets would be connected to adjacent platelets through sintering necks. The alignment of BN platelets was not disrupted by this heat treatment. However, BN platelets tend to form small pieces after sintering at  $1100$  or  $1200 \text{ }^{\circ}\text{C}$  (Figure 3d,f). The sample reduced to almost 50% in dimension when it was sintered at  $1200 \text{ }^{\circ}\text{C}$  with reduced porosity ( $\approx 50\%$ ). Thus, the amount of epoxy impregnated into this structure was significantly lower. Moreover, an oxide layer was formed on the BN surface after sintering at  $1100$  or  $1200 \text{ }^{\circ}\text{C}$ , which in turn influenced on their thermal properties. The formation of the oxide layer was also confirmed from the XRD studies, which is shown in the supporting information (Figure S3, Supporting Information). However, a  $\text{BN}_{\perp}$ - $\text{BN}_{\perp}$ -elaborated and diffused interface was obtained (Figure 3b) (with much lower shrinkage ( $\approx 10\%$ ), and a negligible oxide layer after sintering at  $1000 \text{ }^{\circ}\text{C}$ . Thus, the sintering temperature was optimized at  $1000 \text{ }^{\circ}\text{C}$  to get this aligned BN-BN continuous network, which improved the thermal properties of the composite significantly (discussed in the next section). It is known that the heterogeneous transfer of phonons through the anisotropic filler composites, especially on the filler-resin interface, leads to a large interface resistance and thereby reduced thermal conductivity.<sup>[28]</sup> This well-aligned elevated and continuous  $\text{BN}_{\perp}$ - $\text{BN}_{\perp}$  filler network, where one platelet tends to join with another after sintering, helps to pass the phonon through a faster and effective heat transfer channel by reducing the interfacial resistance. To verify this, the interfacial thermal resistance of the composites, where  $\text{BN}_{\perp}$ - $\text{BN}_{\perp}$  aligned structures were sintered at  $600$  and  $1000 \text{ }^{\circ}\text{C}$ , were calculated using nonlinear Foygel model,<sup>[40]</sup> which can be given by

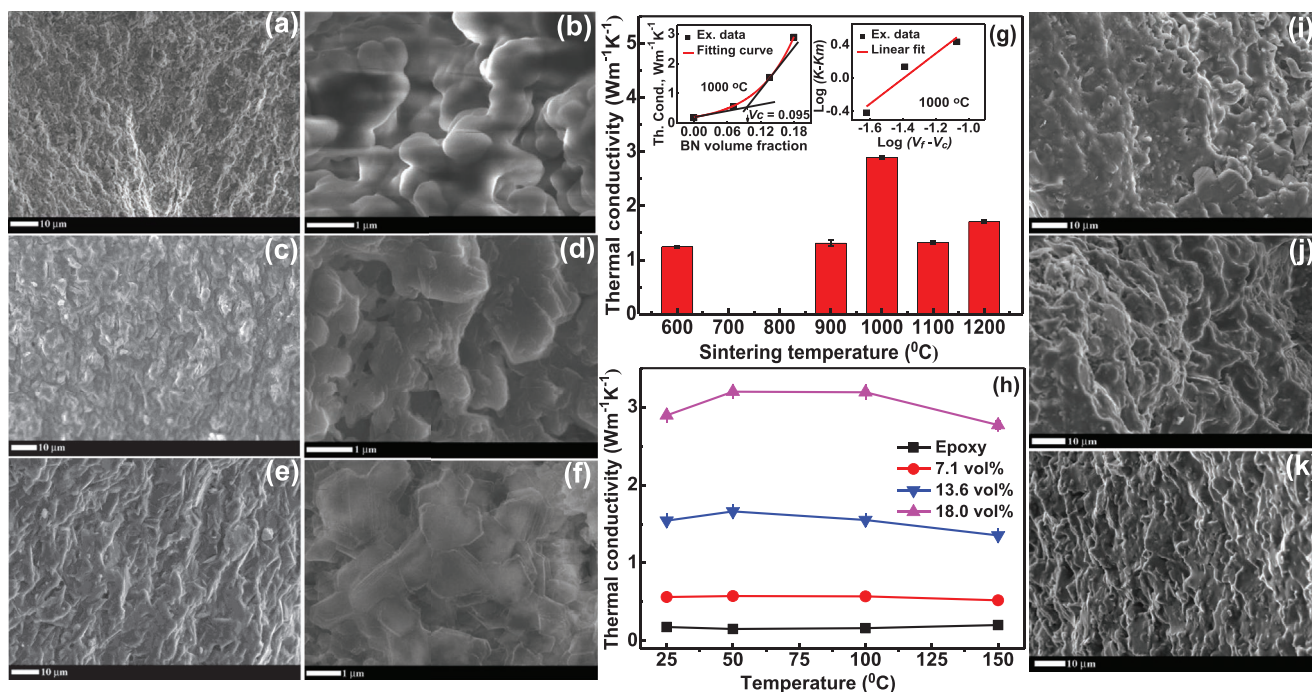


**Figure 3.** Cross-sectional SEM image of BN aligned structures using 5 μm BN platelets after sintering at a,b) 1000 °C; c,d) 1100 °C; and e,f) 1200 °C. b,d,f) High-resolution images of (a), (c), and (e), respectively, showing BN<sub>⊥</sub>-BN<sub>⊥</sub> continuous network due to high-temperature sintering. g) *K* at 25 °C of epoxy/BN composites when aligned structures were sintered at different temperatures (600, 900, 1000, 1100, and 1200 °C) at 18 vol% loading. Left inset of (g) shows fitting experimental thermal conductivity of epoxy/BN composites when the BN<sub>⊥</sub>-BN<sub>⊥</sub> aligned structures were sintered at 1000 °C based on the critical percolation law, and right inset of (g) shows the fitting process of the Foygel model ( $\log(V_f - V_c)$ ) plotted against  $\log(K - K_m)$  for the corresponding composite when the aligned BN structures were sintered 1000 °C. h) *K* as a function of temperature of three epoxy/BN composites along with pure epoxy when aligned BN structure was sintered at optimized temperature, i.e., at 1000 °C. i–k) Cross-sectional SEM images of epoxy/BN composites when aligned structure was sintered at 1000 °C at three different BN loadings, i.e., 7.1, 13.6, and 18.0 vol%, respectively.

$$K - K_m = K_0 \left[ \frac{V_f - V_c}{1 - V_c} \right]^\beta \quad (1)$$

where *K* and *K<sub>m</sub>* are the thermal conductivities of the composites and matrix, respectively. *K<sub>0</sub>* is a preexponential factor ratio related to BN platelets contribution, and β is the conductivity exponent that depends on the aspect ratio of BN platelets. *V<sub>c</sub>* is the critical percolation BN volume fraction, and *V<sub>f</sub>* is the BN volume fraction. After the tangent on the experimental data curve was determined, the value of *V<sub>c</sub>* ≈ 0.095 (shown in the left inset of Figure 3g) for aligned composites with the sintering temperature of 1000 °C was obtained. Equation (1) was then transformed into a linear form:  $\gamma = A + Bx$ , where *A* equals to  $\log K_0$ , *B* equals to β, *x* equals to  $\log [(V_f - V_c)/(1 - V_c)]$ , and γ equals to  $\log(K - K_m)$ . The values of *K<sub>0</sub>* (26.94) and β (1.51) were then derived by fitting experimental data as shown in the Supporting Information (right inset of Figure 3g) for 1000 °C sintered composites. The values of *K<sub>0</sub>* (18.04) and β (1.27) for 600 °C sintered composites were obtained via the same method. The contact resistance (*R*) then can be calculated from the following equation

$$R = \frac{1}{K_0 D V_c^\beta} \quad (2)$$

where *D* (≈120 nm) is the average thickness of BN platelets. Thus, the contact resistance calculated from Equation (2) was  $2.29 \times 10^6$  K W<sup>-1</sup> for 1000 °C sintered composites. The average overlap area between two adjacent BN platelets in aligned structures was calculated using the following equation<sup>[41,42]</sup>

$$A_s = \frac{2D^2}{\pi} \sigma(p) \quad (3)$$

where

$$\sigma(p) = \ln \left[ \frac{\sqrt{1+p^{-1}} + \sqrt{1-p^{-1}}}{\sqrt{1+p^{-1}} - \sqrt{1-p^{-1}}} \right] \quad (4)$$

where *p* is the aspect ratio (*L/D*) of BN platelets. Using Equations (3) and (4), the average overlap area (*A<sub>s</sub>*) between two adjacent BN platelets was calculated ( $4.05 \times 10^{-14}$  m<sup>2</sup>). Finally, interfacial thermal resistance (*R<sub>c</sub>*) was obtained by multiplying the contact resistance (*R*) and average overlap area (*A<sub>s</sub>*), which was obtained from Equations (3) and (4), respectively. The *R<sub>c</sub>* value of BN<sub>⊥</sub>-BN<sub>⊥</sub> aligned structures when sintered at 1000 °C was  $9.27 \times 10^{-8}$  m<sup>2</sup> K W<sup>-1</sup>. This obtained *R<sub>c</sub>* was lower than previously reported study of BN aligned structures by Hu et al.<sup>[28]</sup> It was interesting to note that *R<sub>c</sub>* of 1000 °C sintered epoxy/BN aligned composites was one order of magnitude smaller than

$R_c$  of 600 °C sintered composites ( $3.65 \times 10^{-7} \text{ m}^2 \text{ K W}^{-1}$ ), thus a higher thermal conductivity was expected when aligned structures were sintered at 1000 °C.

To study the effect of interfacial thermal resistance as obtained from the Foygel model due to high-temperature sintering on thermal conductivity, several epoxy/BN composites with similar BN loadings (18 vol%) were prepared, where aligned BN structures were sintered at 600, 900, 1000, 1100, and 1200 °C prior to epoxy infiltration and their thermal conductivity was compared. The comparison of thermal conductivity of the composites at 25 °C where different sintering temperatures were used to form continuous BN aligned networks is shown in Figure 3g. As expected, the highest thermal conductivity was achieved when aligned structures were sintered at 1000 °C due to lower interfacial resistance. The lower sintering temperature (600 °C) may form very little elaborated interface at the BN/BN junction, and thus leads to lower thermal conductivity. At higher sintering temperatures (e.g., 1100 and 1200 °C), a lower thermal conductivity was detected. Such an outcome was due to the higher interface resistance since the platelets tend to form small pieces compromising the degree of alignment as already observed from the SEM analyses (Figure 3d,f). Moreover, an oxide layer, formed on the BN surface after sintering at 1100 or 1200 °C, could decrease the conductivity. Figure 3h shows thermal conductivity as a function of temperature for three epoxy/BN aligned composites (7.1, 13.6, and 18.0 vol% of BN loading) sintered at the optimized 1000 °C, along with pure epoxy. The composite having 18.0 vol% BN loading exhibited conductivity of  $2.85 \text{ W m}^{-1} \text{ K}^{-1}$  at 25 °C, thus an enhancement of almost 1500% with respect to pure epoxy was achieved. Composite with similar BN loading (17.5 vol%) showed conductivity of  $1.25 \text{ W m}^{-1} \text{ K}^{-1}$  at 25 °C (Figure 2f), when aligned BN structures were only sintered at 600 °C. Hence, the higher sintering temperature of 1000 °C exhibited significant improvement in thermal conductivity ( $K$  increased from 600% to 1500%) of the composite. A comparison between the thermal conductivity of the pre-sintered and post-sintered (at 1000 °C) composites with different hBN loadings is shown in Figure S4, Supporting Information. The cross-sectional SEM images of epoxy/aligned BN composites (at 7.1, 13.6, and 18.0 vol% of BN loading) also revealed a straight alignment of BN platelets even after epoxy infiltration, as shown in Figure 3i–k, respectively. Negligible deformation occurred during epoxy infiltration under vacuum, because of stable and strong continuous structures of BN. This continuous network of BN also showed a good wettability and compact interface with resin matrix. In this composite, heat flow would directly transfer to surrounding through the continuous network of diffused  $\text{BN}_\perp$ – $\text{BN}_\perp$  interfaces and thus avoid the jump of phonon at filler/polymer interfaces. Therefore, compared to the traditional filler reinforced matrix, the interfacial thermal resistance of composites with continuous BN networks decreased significantly and thus thermal conductivity of the composites increased by 1500%.

To further improve the thermal properties of composites, the addition of BN nanoparticles was considered for thermal transport junctions when preparing the aligned BN structures. These BN nanoparticles were used to create a linkage between BN micro-platelets after sintering so that a continuous thermal

path was formed, in which the phonon will experience much lower interfacial resistance during propagation. BN platelets with different sizes (BN 30  $\mu\text{m}$  and BN 70 nm), with a variation in mixing ratio by weight (BN 30  $\mu\text{m}$ /BN 70 nm = 2:1, 6:1, 10:1, 12:1, and 17:1) was considered. The cross-sectional SEM images of aligned BN structures using only 30  $\mu\text{m}$  BN platelets, 30  $\mu\text{m}$  BN platelets and 70 nm BN at a 2:1 ratio, and the corresponding composite of mixed BN fillers are shown in Figure 4a–c, respectively. The alignment of fillers was clearly observed along the ice crystal growth direction when using the larger (30  $\mu\text{m}$ ) platelets, as illustrated in Figure 4a. A similar alignment was also detected when using smaller platelets ( $\approx 5 \mu\text{m}$ ), as shown in Figure 2a. In the mixed BN aligned structure (Figure 4b), it was seen that BN nanoparticles were in between two micro-platelets. The concept of using nanoparticles was to create a linkage between neighboring micro-platelets to form a continuous network after sintering. The nanoparticles were hardly seen after sintering because of the formation of an elevated interface. The microstructure of epoxy/mixed BN composite, as shown in Figure 4c, keeps the alignment of BN continuous networks unchanged even after epoxy infiltration without any evident voids and gaps.

To study the effect of the addition of BN nanoparticles (70 nm) into BN micro-platelets (30  $\mu\text{m}$ ) on the thermal properties of the composites, a comparison of thermal diffusivity (at 25 °C and 20 vol% total filler loading) with a different mixing ratio of total BN fillers is shown in Figure 4d. The highest diffusivity was achieved when the weight ratio of BN 30  $\mu\text{m}$  to BN 70 nm equal to 12:1 was considered. When the ratio was higher than 12:1, diffusivity was reduced because of insufficient number of nanoparticles for the larger platelets to join with each other. For a ratio lower than 12:1, smaller number of larger platelets limited the linkage among the fine particles, which may increase the interface resistance. Thus, an optimal ratio of 12:1 (BN 30  $\mu\text{m}$  to BN 70 nm) was chosen for achieving the highest enhancement in the thermal conductivity of the composites. The thermal conductivity of epoxy/BN composite using the optimal mixing ratio of 12:1, along with composite using only 30  $\mu\text{m}$  BN, at 32 vol% total filler loading, is shown in Figure 4e. The mixed BN composite exhibited the conductivity of  $3.60 \text{ W m}^{-1} \text{ K}^{-1}$  at 25 °C,  $4.11 \text{ W m}^{-1} \text{ K}^{-1}$  at 50 °C, and  $4.38 \text{ W m}^{-1} \text{ K}^{-1}$  at 100 °C, whereas  $K$  was 3.50, 3.99, and  $4.19 \text{ W m}^{-1} \text{ K}^{-1}$  at 25, 50, and 100 °C, respectively, when using 30  $\mu\text{m}$  BN only. Summarizing, the enhancement in  $K$  due to this addition of nanoparticles was 2.8% at 25 °C, 3.0% at 50 °C, 4.5% at 100 °C, and 13.6% at 150 °C.

The electrical insulation of the composites was studied by measuring the volume resistivity of the composites along with pure epoxy. All the composites (epoxy/BN random, aligned, and epoxy/mixed BN) along with pure epoxy exhibited a volume resistivity of almost  $10^{14} \Omega \text{ cm}$ , which is shown in the inset of Figure 4e. There were no significant changes in volume resistivity observed between random and aligned composites, even in mixed BN composites. The measured volume resistivity is five orders of magnitude higher than the critical resistance for electrical insulation ( $10^9 \Omega \text{ cm}$ ). Thus, the developed composites have potential applications in thermal management for power electronics, LED packaging, and other fields.

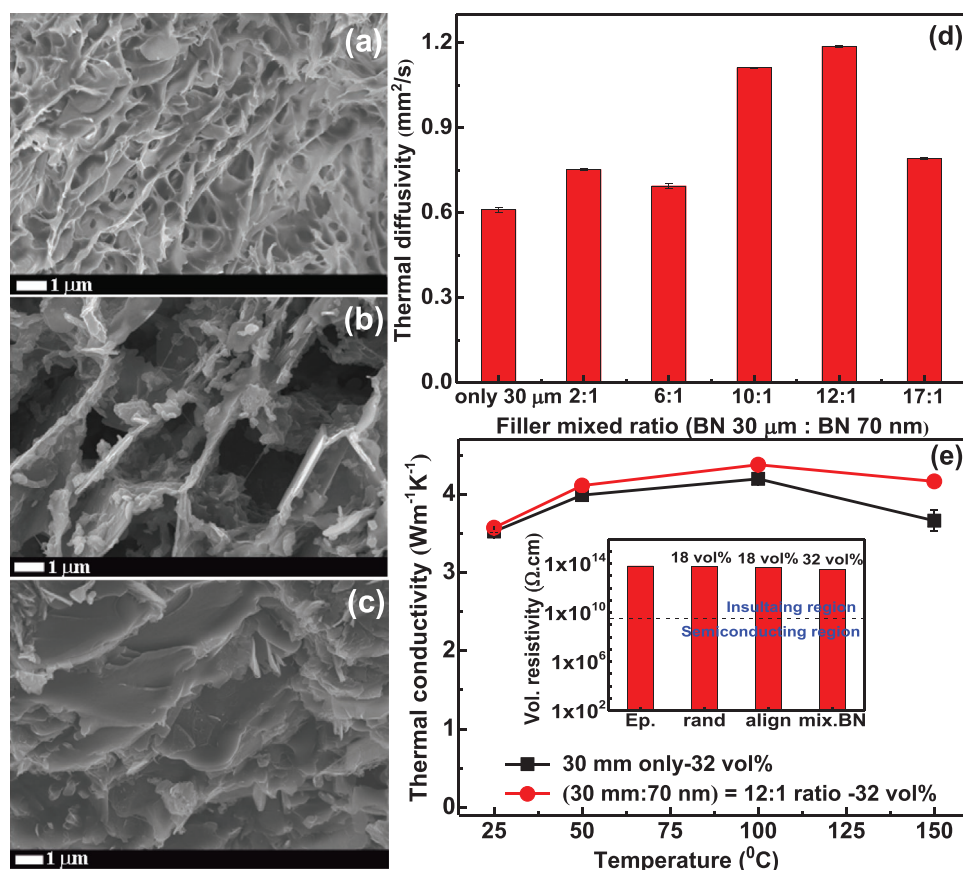


**Figure 4.** Cross-sectional SEM image of a) BN aligned structures using  $\approx 30 \mu\text{m}$  platelets, b) BN aligned structures using  $30 \mu\text{m}$  platelets and  $70 \text{ nm}$  platelets taken as 2:1 ratio, and c) corresponding epoxy/mixed BN composite. d) Comparison of thermal diffusivity of epoxy/BN composites where different mixing ratio (by weight) of BN micro-platelets to BN nanoparticles was used (BN  $30 \mu\text{m}$ /BN  $70 \text{ nm}$  = from 2:1 to 17:1) at  $25^\circ\text{C}$  and 20 vol% of total filler loading. e)  $K$  as a function of temperature of epoxy/BN composite (32 vol% loading) using only  $30 \mu\text{m}$  BN and epoxy/BN composite using  $30 \mu\text{m}$  BN plus  $70 \text{ nm}$  BN (mixing ratio equal to 12:1) with similar total loading. Inset of (e) shows the volume resistivity of pure epoxy along with epoxy/BN random and aligned composites.

A filler arrangement inside a polymer matrix was successfully designed for the development of high thermal conducting composites. This aim was achieved by combining freeze-casting and high-temperature sintering methods. Highly ordered  $\text{BN}_\perp\text{-BN}_\perp$  stacking structures were obtained by the freeze-casting followed by high-temperature sintering at  $1000^\circ\text{C}$ . The BN platelets were aligned along the ice crystal growth direction, where the crystalline structure was preferentially orientated along (100) plane. The high-temperature ( $1000^\circ\text{C}$ ) sintering indicated an advancement over low temperature ( $600^\circ\text{C}$ ) treatment for polyvinyl alcohol (PVA) removal from aligned BN structures. The high-temperature sintering not only removed PVA, but also formed a continuous  $\text{BN}_\perp\text{-BN}_\perp$  interface, with reduced interfacial resistance (interfacial resistance was one order of magnitude lower in  $1000^\circ\text{C}$  sintered composites than  $600^\circ\text{C}$ ), and thus an improved thermal conductivity was obtained. The addition of hBN nanoparticles into bigger platelets acted as thermal transport junctions and further improved the conductivity. An optimal amount of hBN nanoparticles promoted composite's conductivity due to linkage between bigger platelets after sintering and formed a continuous channel with much reduced interfacial thermal resistance. The electrical insulation of the

composites was suitable to be used in thermal management for power electronic device applications.

### 3. Conclusions

A thermally conductive network based on BN was successfully designed for the development of highly thermally conducting composites. Aligned and continuous  $\text{BN}_\perp\text{-BN}_\perp$  stacking structures were obtained by the freeze-casting method followed by high-temperature sintering. All the aligned BN structures are porous and highly anisotropic along the freezing direction. Texture analysis from the XRD studies indicated an increase of  $T_{C(100)}$  from 0.21 to 1.22 in aligned BN structures that further confirmed the preferred orientation of BN platelets towards (100) diffraction plane. The epoxy/BN aligned composites showed 73% improvement in thermal conductivity at 17.5 vol% over randomly distributed BN in epoxy composites. The sintering effect formed an elaborated  $\text{BN}_\perp\text{-BN}_\perp$  diffused interface and ensured the continuity of thermal conducting paths inside the composites. The sintering temperature was optimized to  $1000^\circ\text{C}$ , where

the composites showed significant improvement in thermal conductivity ( $K$  increased from 600% to 1500%, when the sintering temperature increased from 600 to 1000 °C) due to lower interfacial resistance ( $3.65 \times 10^{-7} \text{ m}^2 \text{ K W}^{-1}$  for 600 °C treated composites and  $9.27 \times 10^{-8} \text{ m}^2 \text{ K W}^{-1}$  for 1000 °C sintered composites). The highest achieved thermal conductivity was  $2.85 \text{ W m}^{-1} \text{ K}^{-1}$  at 18.0 vol% BN loading using 5  $\mu\text{m}$  BN platelets. The lower sintering temperature ( $\approx 600$  °C) formed very little diffuse interface at BN/BN junction, thus leading to lower conductivity. At a sintering temperature higher than 1000 °C, the platelets started to form small pieces compromising the degree of alignment. The addition of 70 nm hBN particles into 30  $\mu\text{m}$  platelets was considered for thermal transport junctions to form a continuous thermally conducting network to further improve the conductivity. These BN nanoparticles were used to create an effective linkage between neighboring micro-platelets after sintering. The highest thermal diffusivity was achieved when the weight ratio of BN 30  $\mu\text{m}$  to BN 70 nm was equal to 12:1. Thus, with this optimal amount of hBN nanoparticles (BN 30  $\mu\text{m}$  to BN 70 nm = 12: 1), the composite's conductivity was further increased to  $4.38 \text{ W m}^{-1} \text{ K}^{-1}$  at 32 vol% total filler loading. All composites studied here maintained good electrical insulation (volume resistivity  $\approx 10^{14} \Omega \text{ cm}$ ). The proposed method provides a new concept for future designs of thermally conductive polymer-based composites to be employed in electronic packaging and power electronic applications.

#### 4. Experimental Section

**Materials:** Hexagonal BN platelets with three average diameters ( $\approx 0.07$ , 5, and 30  $\mu\text{m}$ ) were purchased from M.K. Impex Corp. The two-part epoxy resin (low-viscosity, crystal-clear epoxy from East EverLast brand) was used as a polymer matrix. PVA, which was used as an organic binder, was obtained from Sigma-Aldrich.

**Composites Development:** The BN aqueous slurries were first prepared by mixing different BN platelets in an aqueous solution and PVA. The PVA served as bridges to link BN platelets. Highly ordered/aligned BN structures with different densities were fabricated by controlled anisotropic freezing of these BN aqueous slurries. A schematic illustration of preparation of the composite is shown in Figure 1. The composite development process consisted of five steps: 1) preparation and pouring of aqueous slurry containing BN platelets and PVA into mold; 2) freezing of aqueous suspension to form the ice crystals along the temperature gradient; 3) freeze-drying to remove the ice and to obtain porous BN aligned structures; 4) sintering this ordered structures to develop a continuous and diffused  $\text{BN}_{\perp}$ - $\text{BN}_{\perp}$  interface; and finally 5) performing liquid epoxy infiltration under vacuum to derive the composites. Anisotropic freezing using liquid nitrogen was conducted by pouring the aqueous slurry into a mold, which was laid on a copper disk for 3 h to create a temperature gradient and hence to form the ice crystals. The temperature gradient was created along the  $z$ -direction. The water in slurries was frozen from the bottom to top surface (along the temperature gradient) during the directional freezing, and the ice crystals grew vertically. The BN platelets were compressed between two growing crystals and restacked to form interconnected networks. Frozen samples were freeze-dried (Labconco) at low temperature ( $-55$  °C) and pressure (0.018 mbar) for 48 h to obtain porous and aligned BN structures. In freeze-drying process, the ice crystals are sublimed, leaving behind the vertically aligned pores to form highly anisotropic structures. The pore dimensions in the structures can be tuned by changing the directional freezing rate.<sup>[43]</sup> Several BN aligned structures, with different

density values, were prepared by tuning the hBN content in the slurry. PVA was removed when sintering the aligned structures at 1000 °C. This high-temperature sintering of the aligned hBN structures was carried out using a high-temperature laboratory furnace (HTF 1700) at ambient pressure. Using a programmable controller, first a temperature ramp ( $10$  °C  $\text{min}^{-1}$ ) was set up to reach the desired temperature, i.e., 1000 °C, then the samples were sintered in the furnace for 30 min and finally the furnace was cooled down to room temperature with a ramp of  $10$  °C  $\text{min}^{-1}$ . The aligned structure was well maintained even after sintering, as the ratio of BN to PVA, which plays an important role, was kept at 3:1. This high-temperature sintering not only removed the PVA from the aligned structures but also allowed sufficient diffusion between BN particles to form continuous heat conducting paths. Thus, there was no PVA left in the composites, and it did not affect the thermal conductivity calculation of epoxy/BN composites. The density of BN scaffolds was controlled by adjusting the concentration of BN in the solution. The epoxy resin and the curing agent were then uniformly mixed at 3:1 weight ratio at room temperature using a hand mill mixer. Aligned BN skeletons were then completely immersed in the mixture solution. After infiltration, the composite was placed in a vacuum oven at 70 °C to remove trapped air. The liquid epoxy resin was successfully impregnated into BN scaffolds due to capillary force and low-pressure environment. Finally, the composite was cured at 90 °C for 1 h. Extra epoxy that adhered to the composite surface was removed after curing. The volume fraction of the composites was determined based on the weight before and after infiltration of epoxy. For comparison, randomly distributed hBN/epoxy composites at similar loading were also prepared by directly dispersing the hBN into the epoxy (without any PVA). It was hard to control the volume fraction of the sintered BN infiltrating with epoxy, specifically when compared with random composites. The vol% of hBN was adjusted by tuning the hBN content in the initial slurry. Once a certain filler loading was obtained, random composite was prepared with identical loading to compare. Composites with higher hBN vol% may lead to certain pores that were not filled. To avoid this issue, the viscosity of the resin was adjusted by the addition of 1–5 wt% xylene during impregnation into the sintered hBN scaffolds. The maximum porosity (5.4%) was obtained in aligned and sintered hBN/epoxy composites at 32 vol% loading.

**Microstructural and Thermal Analysis:** Scanning electron micrographs were obtained using a JEOL 7100F field-emission gun scanning electron microscope (FEG-SEM). A working distance of 10 mm was maintained utilizing a beam voltage of 10 kV. Crystallographic structures, preferred orientation, were assessed using a Bruker D8 ADVANCE XRD spectrometer, utilizing a parallel beam geometry and glancing angle beam parameters as follows: Cu  $K\alpha$  source,  $\lambda = 1.5406$  Å, 40 kV, and 35 Ma. The XRD of the samples was taken along the ice crystal growth direction, i.e., along the oriented hBN platelets. As some platelets may not be perfectly vertically aligned, thus when taking XRD along the ice crystal growth direction, some other diffraction planes like (102) were also observed due to the alignment of platelets in an angle to  $z$ -direction temperature gradient. XRD traces were measured over a  $2\theta$  range of  $10$ – $60^\circ$ , with a step size of  $0.015^\circ$  ( $2\theta$ ). Relative peak intensities were calculated from the Bruker DIFFRAC.EVA software, and the texture coefficient values were obtained using the Harris equation<sup>[44]</sup>

$$X_C(h,k,l)_i = \frac{I_m(h,k,l)_i}{I_0(h,k,l)_i} \left[ \frac{1}{n} \sum_{i=1}^n \left( \frac{I_m(h,k,l)_i}{I_0(h,k,l)_i} \right) \right]^{-1} \quad (5)$$

where  $I_m$  is the measured diffraction intensity,  $I_0$  is the diffraction database intensity value, and  $n$  is the number of peaks being calculated, in this case  $n = 3$ . Note that the measurements were taken along the ice crystal growth direction. A NETZSCH LFA 467 HyperFlash facility was used to analyze the thermal conductivity,  $K$  of the composites from 25 to 150 °C, using a specimen size of  $10 \times 10$  mm and a thickness of  $\approx 2.5$  mm by the following equation

$$K = \alpha \cdot C_p \cdot d \quad (6)$$



where  $\alpha$  is the thermal diffusivity,  $C_p$  is the specific heat measured by a differential scanning calorimetry (DSC) (model no: TA DSC2500), and  $d$  is the density of the composites calculated from the Archimedes' principle. The coefficient of thermal expansion (CTE) of the composites was measured using thermomechanical analyser (TMA) (model no. Q400 TMA) with a preloaded force of 0.02 N with a 5 °C min<sup>-1</sup> heating rate.

## Supporting Information

Supporting Information is available from the Wiley Online Library or from the author.

## Acknowledgements

This work was supported by the University of Nottingham, Propulsion Futures Beacon project under grant number PF016. The authors acknowledge the use of facilities at Nanoscale and Microscale Research Centre of the University of Nottingham. This research was supported in part by the Engineering and Physical Sciences Research Council (grant number EP/L022494/1). The copyright line for this article was changed on 9 October 2020 after original online publication.

## Conflict of Interest

The authors declare no conflict of interest.

## Keywords

filler alignments, hexagonal boron nitride, high-temperature sintering, polymer composites, thermal conductivity

Received: June 16, 2020  
Revised: August 27, 2020  
Published online:

- [1] L. Moore, L. Shi, *Mater. Today* **2014**, *17*, 163.
- [2] A. K. Singh, B. P. Panda, S. Mohanty, S. K. Nayak, M. K. Gupta, *Polym. Adv. Technol.* **2017**, *28*, 1851.
- [3] L. Jarosinski, A. Rybak, K. Gaska, G. Kmita, R. Porebska, C. Kapusta, *Mater. Sci.-Pol.* **2017**, *35*, 382.
- [4] S. Ata, C. Subramaniam, A. Nishizawa, T. Yamada, K. Hata, *Adv. Eng. Mater.* **2017**, *19*, 1600596.
- [5] W. L. Song, W. Wang, L. M. Veca, C. Y. Kong, M. S. Cao, P. Wang, M. J. Mezziani, H. J. Qian, G. E. LeCroy, L. Cao, Y. P. Sun, *J. Mater. Chem.* **2012**, *22*, 17133.
- [6] C. Min, D. M. Yu, J. Y. Cao, G. L. Wang, L. H. Feng, *Carbon* **2013**, *55*, 116.
- [7] K. H. Su, C. Y. Su, C. T. Cho, C. H. Lin, G. F. Jhou, C. C. Chang, *Sci. Rep.* **2019**, *9*, 14397.
- [8] I. Bustero, I. Gaztelumendi, I. Obieta, M. A. Mendizabal, A. Zurutuza, A. Ortega, B. Alonso, *Adv. Compos. Hybrid Mater.* **2020**, *3*, 31.
- [9] Z. Q. Kuang, Y. L. Chen, Y. L. Lu, L. Liu, S. Hu, S. P. Wen, Y. Y. Mao, L. Q. Zhang, *Small* **2015**, *11*, 1655.
- [10] H. L. Zhu, Y. Y. Li, Z. Q. Fang, J. J. Xu, F. Y. Cao, J. Y. Wan, C. Preston, B. Yang, L. B. Hu, *ACS Nano* **2014**, *8*, 3606.
- [11] S. Moradi, Y. Calventus, F. Roman, J. M. Hutchinson, *Polymers* **2019**, *11*, 1156.
- [12] J. P. Hong, S. W. Yoon, T. Hwang, J. S. Oh, S. C. Hong, Y. Lee, J. D. Nam, *Thermochim. Acta* **2012**, *537*, 70.
- [13] Z. Q. Shi, M. Radwan, S. Kirihaara, Y. Miyamoto, Z. H. Jin, *Appl. Phys. Lett.* **2009**, *95*, 224104.
- [14] W. Dai, J. Wu, Y. Wang, Y. Song, F. E. Alam, K. Nishimura, C. T. Lin, N. Jiang, *J. Mater. Chem. A* **2015**, *3*, 4884.
- [15] B. Román-Manso, Y. Chevillotte, M. I. Osendi, M. Belmonte, P. Miranzo, *J. Eur. Ceram. Soc.* **2016**, *36*, 3987.
- [16] Y. Q. Guo, G. J. Xu, X. T. Yang, K. P. Ruan, T. B. Ma, Q. Y. Zhang, J. W. Gu, Y. L. Wu, H. Liu, Z. H. Guo, *J. Mater. Chem. C* **2018**, *6*, 3004.
- [17] J. Chen, X. Y. Huang, B. Sun, Y. X. Wang, Y. K. Zhu, P. K. Jiang, *ACS Appl. Mater. Interfaces* **2017**, *9*, 30909.
- [18] O. H. Kwon, T. Ha, D. G. Kim, B. G. Kim, Y. S. Kim, T. J. Shin, W. G. Koh, H. S. Lim, Y. Yoo, *ACS Appl. Mater. Interfaces* **2018**, *10*, 34625.
- [19] H. Shen, J. Guo, H. Wang, N. Zhao, J. Xu, *ACS Appl. Mater. Interfaces* **2015**, *7*, 5701.
- [20] C. Yuan, B. Duan, L. Li, B. Xie, M. Huang, X. Luo, *ACS Appl. Mater. Interfaces* **2015**, *7*, 13000.
- [21] Z. Lin, Y. Liu, S. Raghavan, K. Moon, S. K. Sitaraman, C. P. Wong, *ACS Appl. Mater. Interfaces* **2013**, *5*, 7633.
- [22] C. Yu, J. Zhang, W. Tian, X. Fan, Y. Yao, *RSC Adv.* **2018**, *8*, 21948.
- [23] H. B. Cho, T. Nakayama, Y. Tokoi, S. Endo, S. Tanaka, T. Suzuki, W. Jiang, H. Suematsu, K. Niihara, *Compos. Sci. Technol.* **2010**, *70*, 1681.
- [24] T. Fujihara, H. B. Cho, T. Nakayama, T. Suzuki, W. Jiang, H. Suematsu, H. D. Kim, K. Niihara, J. Blendell, *J. Am. Ceram. Soc.* **2012**, *95*, 369.
- [25] K. Wu, J. C. Fang, J. R. Ma, R. Huang, S. G. Chai, F. Chen, Q. Fu, *ACS Appl. Mater. Interfaces* **2017**, *9*, 30035.
- [26] J. C. Zheng, L. Zhang, A. V. Kretinin, S. V. Morozov, Y. B. Wang, T. Wang, X. Li, F. Ren, J. Zhang, C. Y. Lu, *2D Mater.* **2016**, *3*, 011004.
- [27] J. Liu, W. Li, Y. Guo, H. Zhang, Z. Zhang, *Composites, Part A* **2019**, *120*, 140.
- [28] J. Hu, Y. Huang, Y. Yao, G. Pan, J. Sun, X. Zeng, R. Sun, J. B. Xu, B. Song, C. P. Wong, *ACS Appl. Mater. Interfaces* **2017**, *9*, 13544.
- [29] X. Zeng, Y. Yao, Z. Gong, F. Wang, R. Sun, J. Xu, C. P. Wong, *Small* **2015**, *11*, 6205.
- [30] J. Song, Y. Zhang, *Int. J. Heat Mass Transfer* **2019**, *141*, 1049.
- [31] Y. Yao, Z. Ye, F. Huang, X. Zeng, T. Zhang, T. Shang, M. Han, W. Zhang, L. Ren, R. Sun, J. B. Xu, C. P. Wong, *ACS Appl. Mater. Interfaces* **2020**, *12*, 2892.
- [32] R. Malik, Y. Kim, I. Song, *J. Eur. Ceram. Soc.* **2020**, *40*, 594.
- [33] T. Cho, Y. Kim, *J. Eur. Ceram. Soc.* **2017**, *37*, 3475.
- [34] C. Chen, Y. Xue, Z. Li, Y. Wen, X. Li, F. Wu, X. Li, D. Shi, Z. Xue, X. Xie, *Chem. Eng. J.* **2019**, *369*, 1150.
- [35] P. S. Ho, H. B. Huntington, *J. Phys. Chem. Solids* **1966**, *27*, 1319.
- [36] C. Y. Zhi, Y. Bando, C. C. Tan, D. Golberg, *Solid State Commun.* **2005**, *135*, 67.
- [37] M. Kumar, A. Kumar, A. C. Abhyankar, *ACS Appl. Mater. Interfaces* **2015**, *7*, 3571.
- [38] W. N. dos Santos, J. A. de Sousa, R. Gregorio Jr., *Polym. Test.* **2013**, *32*, 987.
- [39] A. A. Balandin, *Nat. Mater.* **2011**, *10*, 569.
- [40] P. Bonnet, D. Sireude, B. Garnier, O. Chauvet, *Appl. Phys. Lett.* **2007**, *91*, 201910.
- [41] A. P. Wemhoff, *Int. J. Heat Mass Transfer* **2013**, *62*, 255.
- [42] C. Fu, Q. Li, J. Lu, S. Mateti, Q. Cai, X. Zeng, G. Du, R. Sun, Y. Chen, J. Xu, C. P. Wong, *Compos. Sci. Technol.* **2018**, *165*, 322.
- [43] X. Xie, Y. Zhou, H. Bi, K. Yin, S. Wan, L. Sun, *Sci. Rep.* **2013**, *3*, 2117.
- [44] G. B. Harris, *Philos. Mag.* **1952**, *43*, 113.